AD-A068 873 ARTEC ASSOCIATES INC HAYWARD CALIF F/G 20/9
SHOCK PHYSICS OF NONIDEAL PLASMAS.(U)
APR 79 D W BAUM, W L SHIMMIN, R F FLAGG N00014-78-C-0354
UNCLASSIFIED AR-130 NL

| OF |
AD
A068873

END
DATE
FILMED
7-79
DDC

LEVEL II

12

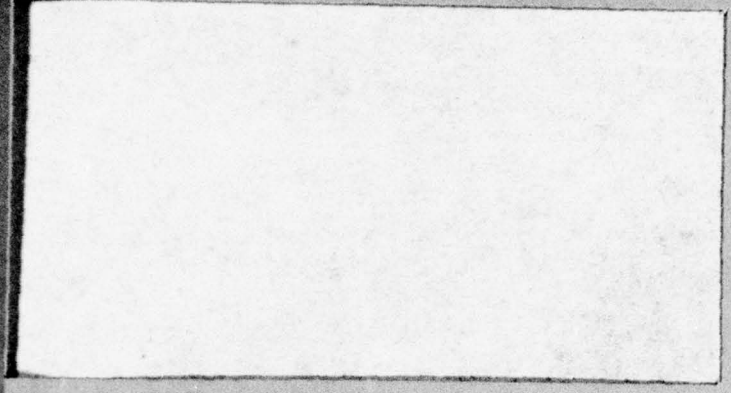

ARTEC ASSOCIATES·INC

79 05 18 064

LEVEL II

12

(6) SHOCK PHYSICS OF NONIDEAL PLASMAS

(14) AR-

Annual Report 130

(11) 30 April 1979

(9) Final Report, 15 March 1978 to 14 April 1979

(12) 64 p.

Sponsored by: Office of Naval Research
Requisition Authority No.
NR 099-408/2-23-78 (473)
Contract No. N00014-78-C-0354

Prepared by: (10) (15) Dennis W. Baum, Stephen P. Gill, W. Lee Shimmin, D. Mukherjee, Robert F. Flagg and John D. Watson

ARTEC ASSOCIATES INCORPORATED
26046 Eden Landing Road
Hayward, California 94545
Telephone: (415) 785-8080

408 296

UNCLASSIFIED

SECURITY CLASSIFICATION OF THIS PAGE (When Data Entered)

REPORT DOCUMENTATION PAGE		READ INSTRUCTIONS BEFORE COMPLETING FORM
1. REPORT NUMBER AR-130	2. GOVT ACCESSION NO.	3. RECIPIENT'S CATALOG NUMBER
4. TITLE (and Subtitle) SHOCK PHYSICS OF NONIDEAL PLASMAS		5. TYPE OF REPORT & PERIOD COVERED Annual Report 15 Mar 78 to 14 Jan 79 6. PERFORMING ORG. REPORT NUMBER
7. AUTHOR(s) Dennis W. Baum, Stephen P. Gill, W. Lee Shimmin, D. Mukherjee, Robert F. Flagg, and John D. Watson		8. CONTRACT OR GRANT NUMBER(s) N00014-78-C-0354
9. PERFORMING ORGANIZATION NAME AND ADDRESS ARTEC ASSOCIATES INCORPORATED 26046 Eden Landing Road Hayward, California 94545		10. PROGRAM ELEMENT, PROJECT, TASK AREA & WORK UNIT NUMBERS 122401
11. CONTROLLING OFFICE NAME AND ADDRESS Office of Naval Research, Dept. of Navy 800 N. Quincy Street Arlington, Virginia 22217		12. REPORT DATE 30 April 1979 13. NUMBER OF PAGES 63
14. MONITORING AGENCY NAME & ADDRESS(if different from Controlling Office)		15. SECURITY CLASS. (of this report) UNCLASSIFIED 15a. DECLASSIFICATION/DOWNGRADING SCHEDULE

16. DISTRIBUTION STATEMENT (of this Report)
Approved for Public Release;
Distribution Unlimited

17. DISTRIBUTION STATEMENT (of the abstract entered in Block 20, if different from Report)

18. SUPPLEMENTARY NOTES

19. KEY WORDS (Continue on reverse side if necessary and identify by block number)
Pulse Power Generation
Explosive Magnetohydrodynamic Generator
High Density Plasmas

20. ABSTRACT (Continue on reverse side if necessary and identify by block number)

This study is an experimental investigation of nonideal plasmas produced by strong shock waves. The study centered about the understanding of factors controlling the specific energy and transport properties of dense plasma in an explosively energized plasma source. The study addressed specifically the gas cavity geometry, pressure-density effects, radial velocity effects, and size scaling. Both argon and xenon were →

next page

DD FORM 1 JAN 73 1473 EDITION OF 1 NOV 65 IS OBSOLETE

UNCLASSIFIED

SECURITY CLASSIFICATION OF THIS PAGE (When Data Entered)

DD Form 1473: Report Documentation Page

SECURITY CLASSIFICATION OF THIS PAGE(When Data Entered)

20. ABSTRACT (Continued)

used for the working gas. Shock speeds ranged from 25.9 to 32.5 km/sec, and measured gas conductivities of 10 to 50 kilosiemens/meter were obtained. The highest peak field amplification in the four shot series was 19 dB.

 UNCLASSIFIED

SECURITY CLASSIFICATION OF THIS PAGE(When Data Entered)

PREFACE

This work was sponsored by the Power Program of the Office of Naval Research with John Satkowski, Director, as technical monitor. His support, comments, and direction are gratefully acknowledged by the authors. Additionally, the advice and support of Dr. E. Florence of the ONR-Pasadena office is also gratefully acknowledged. The genuine interest of these two scientific officers has been instrumental in attaining the accomplishments of this research and is sincerely appreciated by the Artec Associates task team.

The work presented in this report was performed at Artec Associates Incorporated, Hayward, California, by a task team composed of Drs. Dennis W. Baum, Stephen Gill, Deb Mukherjee, Robert Flagg, W. Lee Shimmin, and John D. Watson. Dr. Dennis Baum was the task leader and principal investigator.

TABLE OF CONTENTS

LIST OF FIGURES

LIST OF FIGURES (Continued)

LIST OF TABLES

1. INTRODUCTION

This annual report covers research concerned with increasing our understanding of nonideal dense plasmas produced by strong explosively driven shock waves. The research effort was performed for the Office of Naval Research-Power Program under Contract N000014-78-C-0354, and utilized a novel, high performance explosively driven plasma source.

The plasma conditions produced by these new sources are substantially more energetic and nonideal than those investigated or achieved in earlier programs, and underscore the dearth of knowledge and understanding of dense nonideal plasmas.

The research effort covered in this report consists mainly of four explosively driven plasma source experiments that were designed, fabricated, instrumented, fired, and analyzed during the course of this contract period.

1.1 Background

For several years Artec Associates has been actively engaged in pulsed power generation using an explosively driven MHD concept[1,2,3]. The key element of this novel concept is a plasma source which converts the chemical

energy of an explosive into a very high enthalpy fully ionized plasma. The high density plasma is in turn driven into a channel and through a magnetic field in a MHD section. The electrical output of this section is used to power an augmenting magnetic field intensifying the total magnetic field through self-excitation and ultimately driving an external load.

The concept of a fully self-excited explosive MHD pulse power generator is particularly attractive for many Naval applications. Such a generator, consisting only of explosive, metal tubing and a permanent magnet, would have an attractively long shelf-life. Startup time from initiation to full power is nearly instantaneous, and tens of megajoules of electrical energy are available at gigawatt power levels. These explosive generators are inherently small, and compatible with many special weapon applications. Other applications may well become apparent as the program progresses.

Explosive MHD generators of the externally-excited variety have been experimentally demonstrated many times in the past, but the real progress toward a fully self-excited generator has been thwarted by a lack of knowledge of the properties of dense nonideal plasmas. Measured

electrical conductivities in our experiments for example are substantially less (up to a factor of 10) than calculations based on ideal plasma theory. To compensate for the difference and to still achieve full self-excitation it has been necessary to increase both energy and duration of the explosive plasma source.

1.2 Previous Research Effort

Previous research has been directed toward investigating the shock physics of nonideal plasmas[1], and developing an advanced high-performance plasma source. This effort was quite successful, and Artec Associates conceived an explosive plasma source that was far more energetic than any used before.

The new, high performance explosive plasma source compresses plasma to denser, more nonideal states than before. Much of the energy addition to the plasma occurs at densities exceeding normal solid density for many materials and nonideal effects dominate the plasma behavior.

2. EXPERIMENTAL RESEARCH ON NONIDEAL PLASMAS

2.1 Description of the Plasma Source

A schematic diagram of the plasma source is shown in Figure 1. It is comprised of an annular region of argon gas which is shock-compressed by a detonating explosive. At the end of the cylindrically symmetric annular region, the shocked argon is converged radially into a hemispherical transition section and exhausted into a diagnostic channel located on-axis. This driver configuration was used in three shots, 130-2, 130-3, and 130-4. The conical driver shown in Figure 2 and discussed in previous reports was used to drive Shot 130-1.

The annular portion of the plasma source operates much as the explosive plasma sources described in earlier research reports[1,2,3]. More energy is added to the plasma by the pronounced radial convergence of the flow and explosive compression of the reservoir. In other words, the converging shock flow now stagnates along the axis, forming a much higher pressure, higher density plasma reservoir than previously. Nearly simultaneously, the metal cap at the end of the interior explosive is explosively accelerated and compresses and energizes the plasma even further. As can be appreciated, the convergence, compression, and exhaust processes are all mutually dependent. Timing is critical

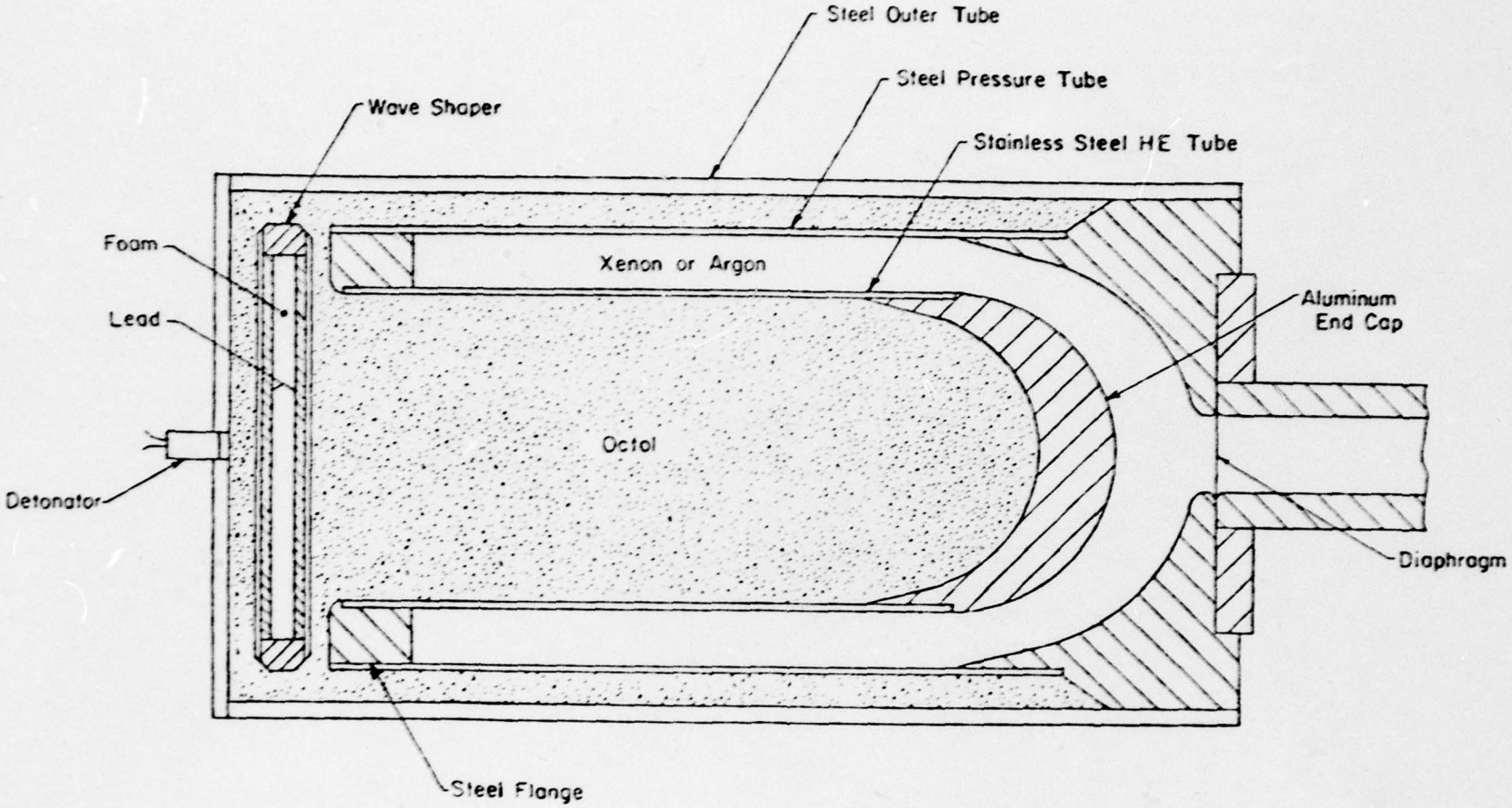

Figure 1 Schematic of Plasma Source for Shots 130-2, 130-3, and 130-4

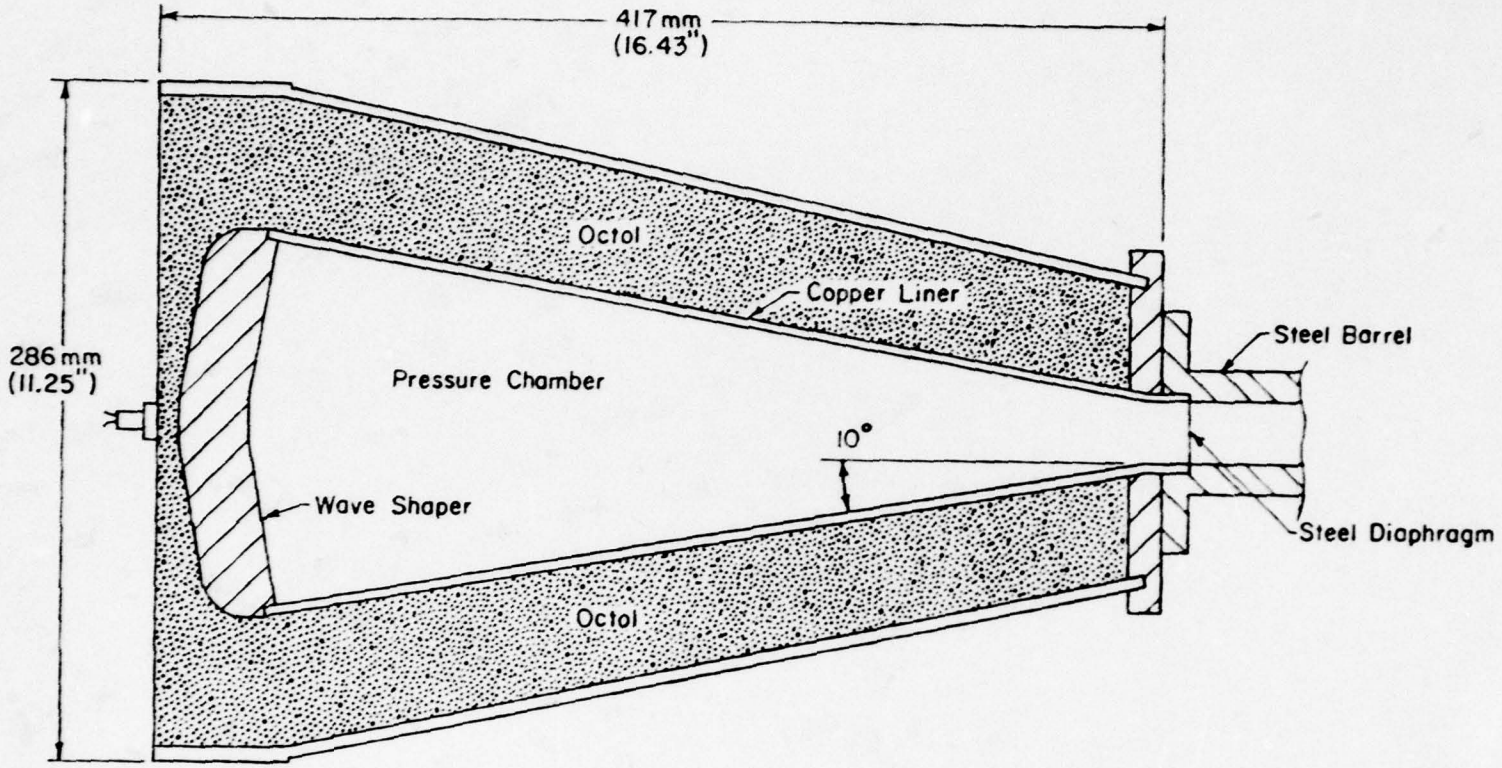

Figure 2 Schematic of Conical Plasma Source for Shot 130-1

in achieving high performance of the plasma source but experimental performance of the plasma source has been very satisfying, even though the design has not yet been optimized.

Overall efficiency, i.e. conversion of explosive chemical energy to useful plasma enthalpy, already exceeds 25%, and will most likely be increased further with design refinements. We note that plasma energy is higher than that achieved in any previous plasma source. MHD channel conditions are also very good, and even with a relatively small diameter driver, a significant degree of generator self-excitation has been achieved. Full self-excitation appears highly probable with a larger source, or with mechanical design refinements.

2.2 Estimate of Nonideal Plasma States

Plasma states achieved in the new plasma source may be estimated from experimental data and the best available nonideal plasma theory[4]. The initial driver shock wave in the annular region of the plasma source has a measured particle velocity of 8.5 km/s (the detonation velocity of Octol). Using this measured velocity and assuming the Debye-Huckel theory with a zero shielding coefficient, the shocked gas conditions are calculated to be: pressure,

3GPa (30 kbar); density, 0.33 Mg/m^3 (g/cm^3); and energy 37 MJ/kg. These estimates are fairly accurate, as the pressure and energy states behind a shock are relatively insensitive to uncertainties in the equation of state. However, the Debye-Huckel plasma theory used in the calculations is about at the limit of credibility because of the dense plasma state.

An estimate of the reservoir entropy state may be calculated assuming a single strong reflected shock. To account for the high density, we have used the empirical Jones-Wilkins-Lee (JWL)[5,6] equation of state commonly used in explosive detonation theory. Calculated conditions for the above initial shock are: pressure, 35 GPa (350 kbar); density, 1.30 Mg/m^3 (g/cm^3); and energy, 80 MJ/kg.

Final compressed state in the reservoir can be estimated assuming an isentropic compression of this stagnated region to a value obtained by matching experimental shock velocity data. For example, the magnitude of the shock velocity in the diagnostic channel is a direct consequence of specific reservoir conditions. By matching the experimental data for shock velocity, a unique value of the reservoir conditions can be obtained. Using this approach, peak plasma conditions in the reservoir were determined to be: pressure,

84 GPa (840 kbar): density, 2.2 Mg/m^3 (g/cm^3); and energy 97 MJ/kg.

Plasma states in the reservoir achieved by the new plasma source are located almost off the edge of the plasma parameter chart, shown in Figure 3, and even the expanded plasma is well into the nonideal region at the right of the plasma parameter chart. The chart and the parameters were described previously in our 1978 research report[1], but key parts will be summarized here. QNTM is the ratio of electron thermal deBroglie wavelength to Debye length. For values greater than 0.1 quantum diffraction effects become important in plasma theory. INTPAR is the plasma nonideal interaction parameter, i.e. the ratio of coulomb electrostatic energy to thermal kinetic energy. Ideal plasma theory assumes INTPAR to be very small. In fact the Debye-Huckel theory, which represents a first order correction to ideal plasma theory, is known to be invalid above an interaction parameter of 0.47. Finally, DGN is the quantum degeneracy parameter, the ratio between electron thermal deBroglie wavelength to electron separation.

It can be seen from the figure that the Artec plasma source yields conditions well into the nonideal plasma regime, indeed much further than the earlier plasma sources. In order to understand the details of the shock energization process, particularly the final compression of the reservoir,

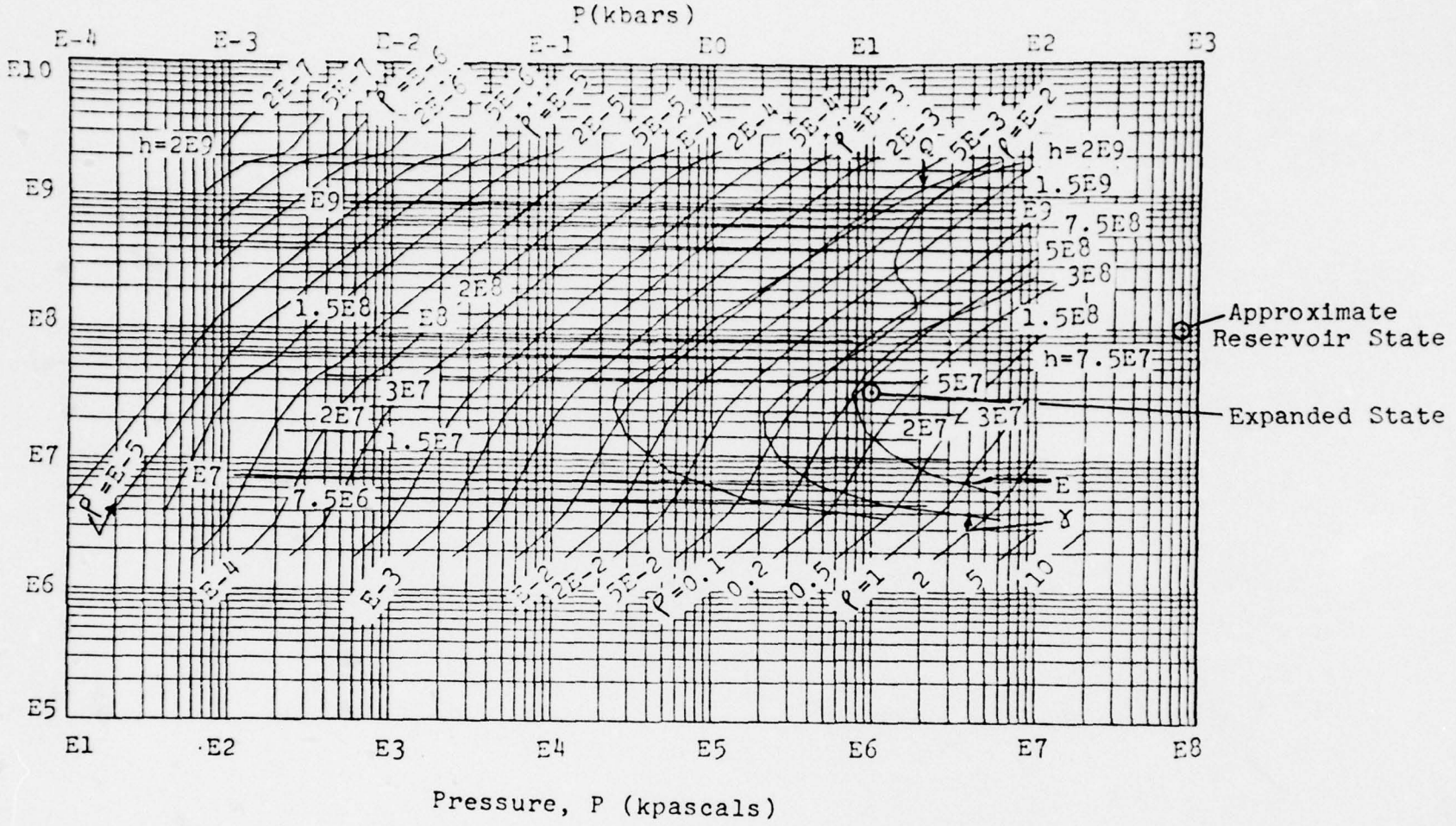

Fig. 3 Plasma Parameter Chart for Argon

it is necessary to have a clear understanding of the physics of strongly nonideal plasmas. Once the plasma expands into the MHD channel, the static pressures drop to about 0.1 GPa (1 kbar), hence the MHD interaction process can be studied using "moderately nonideal" plasma theory.

2.3 Description of the Experimental Apparatus

Four experiments were designed, instrumented and fielded for this contract. The basic design parameters are given in Table 1.

Shot 130-1 utilized a conical driver and xenon gas at 137 kilopascals (20 psia) as the driver gas. The main purpose of this experiment was to fire a conical imploding driver, measure the flow properties of the driver gas as it expanded into a partially evacuated channel, and compare these properties with the expected flow properties based on calculated driver performance.

Shot 130-2 utilized a 17 cm diameter imploding/exploding driver with xenon gas at 694 kilopascals (100 psia) as the driver gas. The main purposes of this experiment were to evaluate this type of driver, to measure the properties of the plasma as it expanded into a partially evacuated channel,

TABLE 1 PLASMA SOURCE PARAMETERS

Shot No.	Plasma Source	Source Diameter	Driver Gas	Initial Pressure in Channel	Explosive	Shock Pressure
130-1	Conical	17 cm	20 grams Xenon	6.65 Kpascals	75/25 Octol	30 Kbars
130-2	Annular	17 cm	55 grams Xenon	6.65 Kilo-pascals	75/25 Octol	30 Kbars
130-3	Annular	17 cm	55 grams Argon	6.65 Kilo-pascals	75/25 Octol	30 Kbars
130-4	Annular	30 cm	302 grams Argon	6.65 Kilo-pascals	75/25 Octol	30 Kbars

and to assess the improvement in performance of this source by comparing the output with the configuration of Shot 130-1.

Shot 130-3 utilized a 17 cm. diameter imploding/exploding driver as before but with argon at 2.12 megapascals as the driver gas. The purpose of this experiment was to fire an imploding/exploding type plasma source using argon and compare the resulting performance with the same configuration using xenon (Shot 130-2). Plasma output was to be assessed using the same diagnostics as Shot 130-2, and in addition a self-excited MHD station was included for additional diagnosis of the plasma parameters.

Shot 130-4 utilized a 30 cm. imploding/exploding driver with argon at 2.07 megapascals as the driver gas. It was felt that the mass of the driver-processed-gas in the 17 cm. diameter drivers was limiting the flow duration of the channel flow to nominally 30 microseconds, and that increasing the outside diameter to 30 centimeters and the mass of the gas by better than fivefold would increase the total flow time to 50 to 60 microseconds, and permit as much as 40 dB magnetic field enhancement.

Additionally, a minor redesign of the field coil to prevent mechanical short circuits was also included on 130-4

to negate suspected shorts which we initially suspected helped to limit the increase in magnetic field in 130-3 to 19 dB.

2.4 Description of the Diagnostics

Shot 130-1: A drawing of the plasma source used in this shot was shown previously in Figure 2. The explosive used was 75/25 Octol; the imploding liner was copper (4.0 mm. or 156 mils thick); the cone half-angle was 10^0; and the charge-to-mass ratio was 3.9. The thick steel wave shaper permitted a single detonator to provide a symmetrical annular detonation front. The cone angle was calculated to produce an axially progressing impact point with a speed of 17 km/s.

The driver gas chamber was loaded with 20 grams of xenon to provide a nominal shock pressure of 2.4 GPa (24 kbar). The diagnostic channel was loaded with air at 6.65 kPa (50 Torr) and was separated from the driver by a thin steel diaphragm.

The layout of the diagnostics in the channel is shown in Figure 4. There was one velocity gage or open circuit voltage measurement and one electrode station with an 11 milliohm load (a thin strip of stainless steel) at which the loaded voltage and current were to be measured. A pair

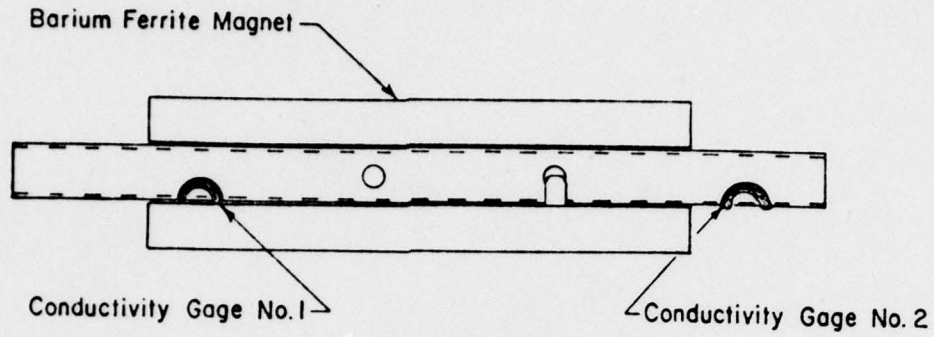

Top View

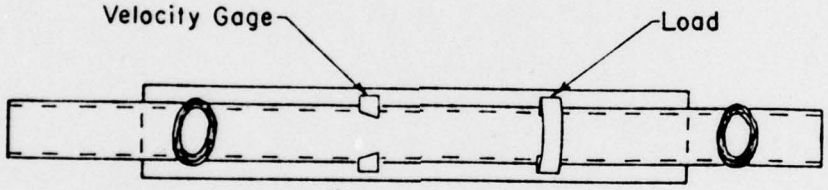

Side View

Figure 4 Layout of Diagnostics for Shots 130-1 and 130-2

of 0.3 meter-long barium-ferrite magnets provided a transverse magnetic field of 77 mT (770 gauss) and 83 mT (830 gauss) at the velocity gage and load stations respectively. There were two conductivity gages, one located near the upstream end of the magnets and one near the downstream end as shown in the figure.

Shot 130-2: A drawing of the plasma source was shown previously in Figure 1. The explosive used was 75/25 Octol. The wave shaper was so configured that a single detonator on-axis provided a symmetric detonation front sweeping along both tubes simultaneously.

The driver gas chamber was loaded with 56 grams of xenon to provide a nominal shock pressure of 3.0 GPa (30 kbar). The diagnostic channel was loaded with air at 6.65 kPa (50 Torr) and was separated from the driver by a 25μm thick stainless steel diaphragm.

The layout of the diagnostics in the channel is shown in Figure 4 and is identical with Shot 130-1. There was one velocity gage or open circuit voltage measurement and one electrode station with an 11 milliohm load (a thin strip of stainless steel) at which the loaded voltage and current were measured. A pair of 0.3 meter-long barium-ferrite magnets provided a transverse magnetic field of

75 mT (760 gauss) and 89 mT (890 gauss) at the velocity gage and load stations respectively. There were two conductivity gages, one located near the upstream end of the magnets and one near the downstream end as shown in the figure.

Shot 130-3: The mechanical configuration of the experiment was the same as Shot 130-2, except that the driver was loaded with argon gas instead of xenon. Nominal shock pressure in the driver was 3.0 GPa (30 kbar) and the diagnostic channel was loaded with air at 6.65 kPa (50 Torr).

The first part of the diagnostic channel, comprising two conductivity gages, a velocity gage, and an MHD load station, was identical to Shot 130-2. The second part of the diagnostic channel included a self-excited MHD generator stage and a third conductivity gage. Experimental layout of the generator section is shown in Figure 5.

A pair of 150 mm. long barium-ferrite magnets provided a transverse mangetic field of 82 mT at the generator location. Flush brass electrodes, 25 mm. long and 80 degrees wide (on a 25 mm. diameter channel) were soldered directly to a one-turn self-excitation coil made from #10 AWG wire braid. Measured inductance and resistance of the field

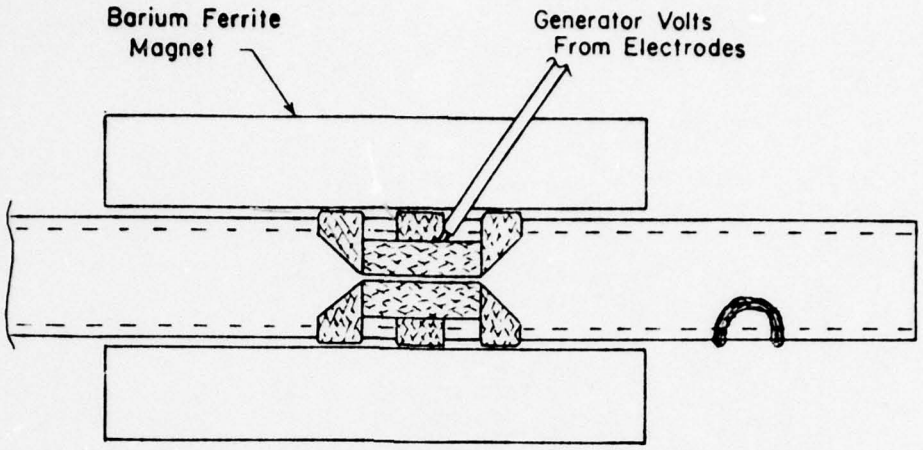

Top View

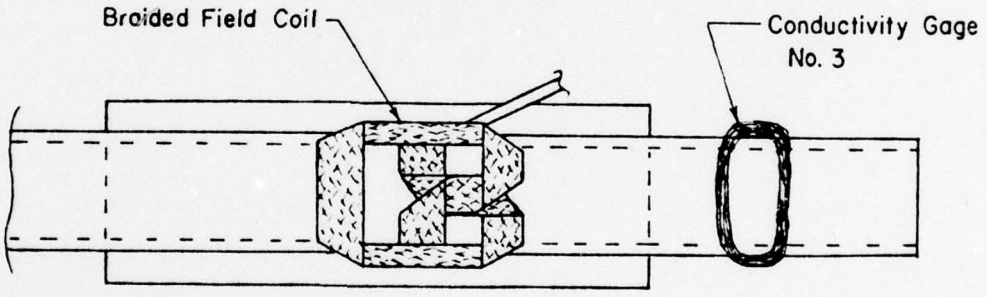

Side View

Figure 5 Layout of Self-Excited Generator Station

coil were 35.9 nanohenries and 0.403 milliohms respectively. Measured B/I ratio at the tube wall was 18.2 microTesla/amp.

Shot 130-4: The geometrical configuration of 130-4 was nearly identical to 130-3 except that the driver outside diameter was increased to 30 centimeters. A full 2X scale up from the baseline 17 centimeters was discarded since tubing of the desired dimensions is not commercially available. The driver gas was argon and the diagnostic channel was loaded with air at 6.65 kilopascals (50 Torr) as previously.

The first section of the diagnostic channel contained 2 side-mounted conductivity gages (gages 1 and 2), a velocity gage and a conventional MHD generator. The magnetic field for these 3 diagnostic tools was provided by two barium-ferrite permanent magnets mounted to produce a B field of .09 Tesla orthogonal to the flow velocity vector.

The second section of the diagnostic channel included a third side-mounted conductivity gage and a self-excited MHD generator stage. The experimental configuration is given schematically in Figure 6.

The initial magnetic field for this section was provided by a pair of barium-ferrite permanent magnets.

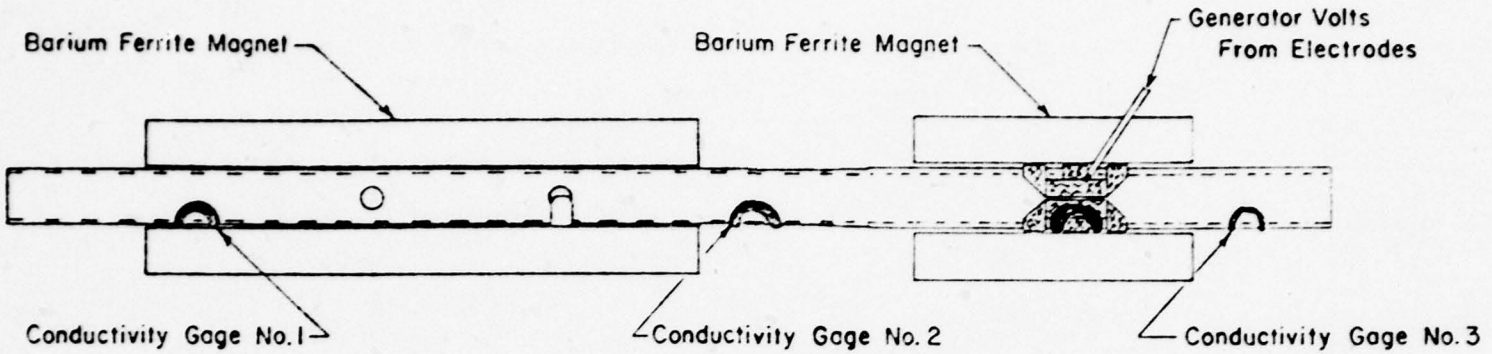

Top View

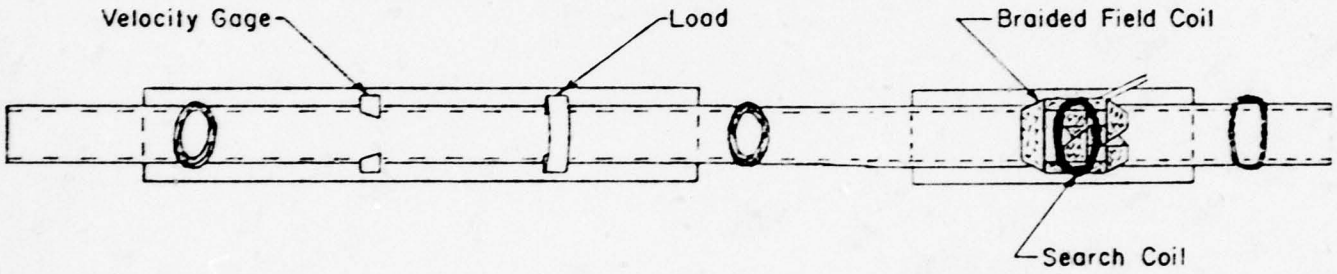

Side View

Figure 6 Channel Layout for Shot 130-4

Additionally, flush brass electrodes were connected to a low inductance one-turn self-excitation coil made from #8 AWG wire braid. The measured inductance of the field coil was 37.9 nanohenries. The D.C. resistance was 0.525 milliohms. The measured B/I at the tube centerline was 24.3 microtesla per amp.

3. RESULTS AND CONCLUSIONS

3.1 Plasma Source Performance

Pairs of symmetrical ionization pins placed on either side of the plasma source reported within fractions of a microsecond of each other, verifying the symmetry of the detonation. The pins also verified the correct (expected) detonation velocity for Octol, 8.48 km/sec. A typical plot of driver ionization pin data is shown in Figure 7. The precision and symmetry of the data is clear from the figure.

In all cases the driver gas initial pressure (hence density) was adjusted to yield 30 kbars static pressure behind the driven initial shock. This nominal or standard condition was used in each case to allow comparing the different cases, one with another.

A flash X-ray photograph of an annular plasma source, shown with the detonation wave approximately half way along the driver, is given in Figure 8. The high degree of symmetry both for the inside and outside collapsing walls and from one side to the other is evident.

In the linear section of the source for 130-2 and 130-3, the total enthalpy was 80.2 MJ/kg giving a total energy of 4.5 MJ for the 56 grams of gas. In the convergent section of the source, which effectively acts as a reservoir, the

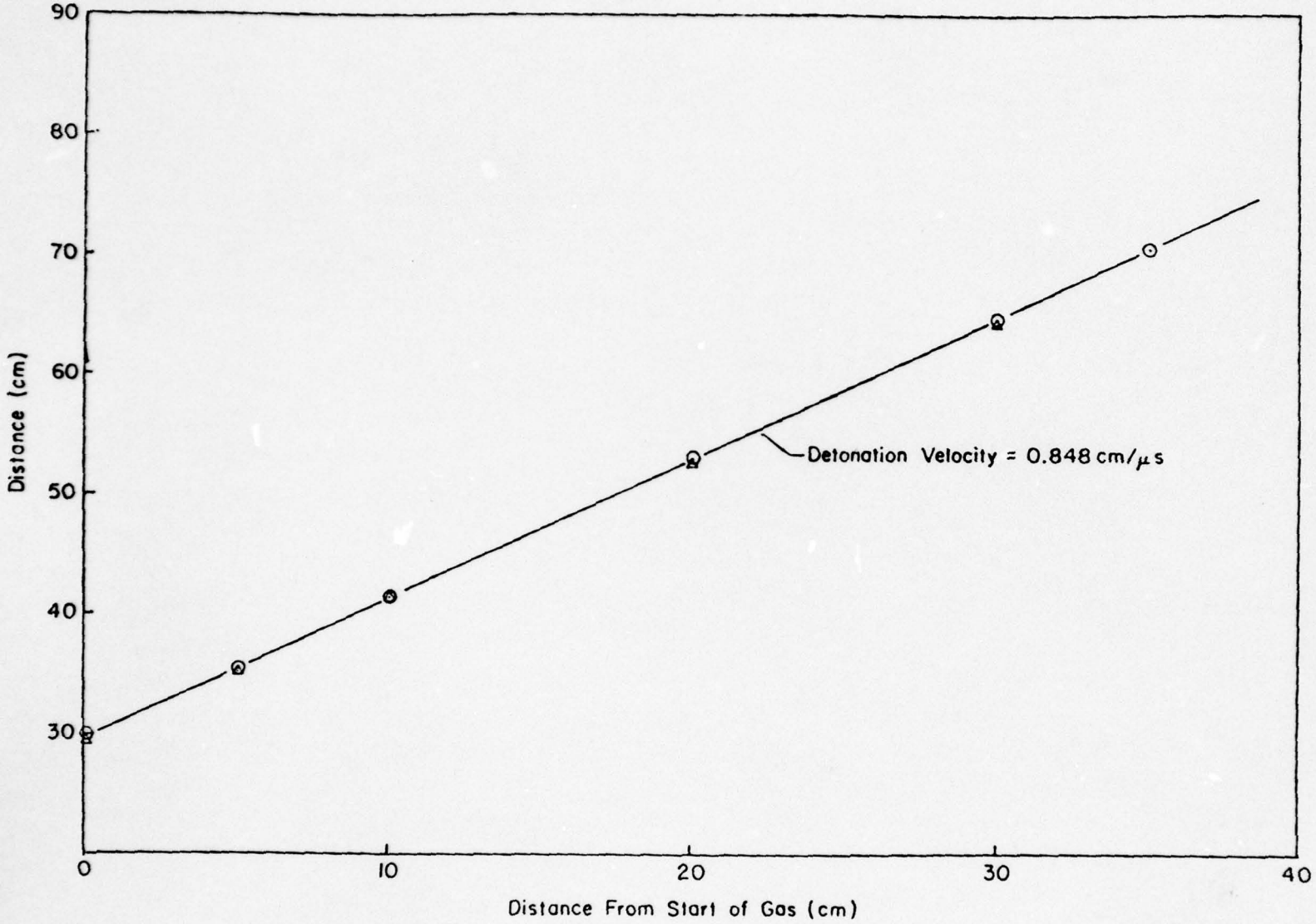

Figure 7 Distance-Time Diagram for Octol Annular Plasma Source (130-4)

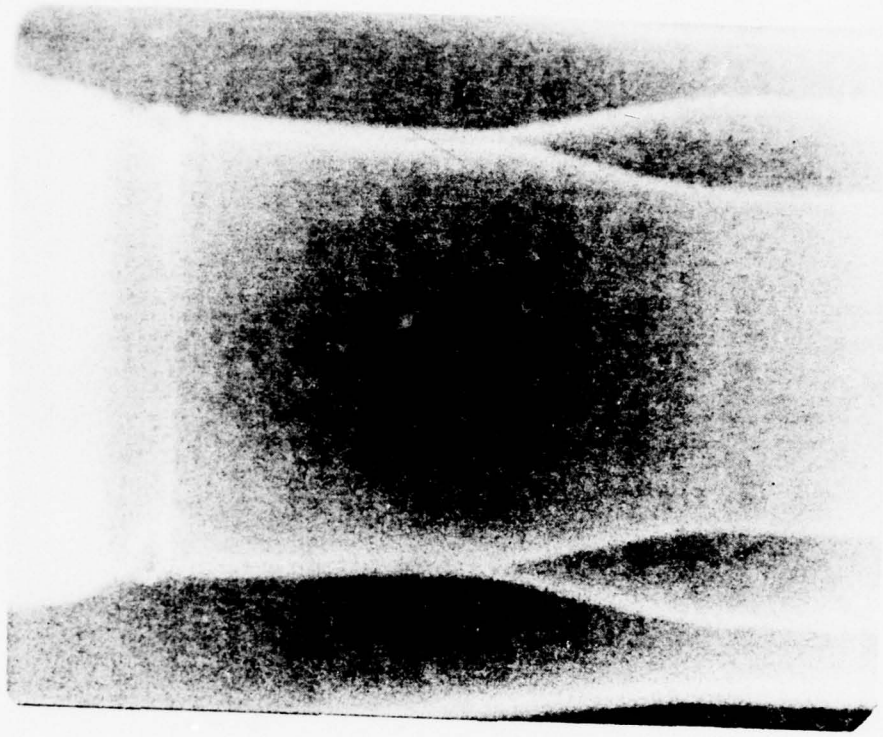

Figure 8 120 MEV Flash Radiograph of a 30 kbar High Efficiency Explosive Plasma Source

total enthalpy is estimated to be 134 MJ/kg. On the assumption that all of the gas achieved this enthalpy, the total energy in the plasma was 7.5 MJ.

3.2 Channel Conditions

The initial pressure in the diagnostic channel in all cases was 6.65 kilopascals (50 Torr) of air, hence the performance of all the sources in terms of the equivalent reservoir conditions produced can be seen from a comparison of the initial shock velocity in the diagnostic channel. These velocities are tabulated in Table 2.

For Shot 130-1, a channel shock speed of 27.3 km/s was obtained from shock front arrival times at the diagnostic stations and from shock breakout at the diaphragm which was monitored by a photodiode. The initial plasma flow velocity calculated from the observed shock velocity is 24.8 km/s. From the velocity gage record the initial flow velocity was measured to be 22.7 km/s, which is 8 percent below the calculated value. Since this particular velocity gage was located five channel diameters downstream of the magnet edge and since the magnetic Reynolds number of the flow was not sufficiently high to cause significant perturbation of the velocity gage reading at that distance, we suspect the source of the discrepancy must lie in other than R_m effects.

TABLE 2 INITIAL SHOCK AND FLOW VELOCITIES

Shot No.	Measured Initial Shock Velocity (km/sec)	Measured Initial Flow Velocity (km/sec)	Calculated Initial Flow Velocity (km/sec)
130-1	27.3	22.7	24.8
130-2	25.9	19.2	23.6
130-3	26.4	20.6	23.6
130-4	32.5	27.3	29.7

For Shot 130-2, a channel shock speed of 25.9 km/s was obtained from shock front arrival times at the diagnostic stations and from shock breakout at the diaphragm, which was monitored by a photodiode. This slightly lower velocity (5 percent compared to the previous shot) is probably within the experimental scatter in the data.

For Shot 130-3, a channel shock velocity of 26.4 km/s was measured, compared to 25.9 km/s in the previous shot, and is essentially the same, implying that, from a shock velocity point of view, argon and xenon drivers are nearly identical in performance.

A channel shock velocity of 32.5 km/s was measured for Shot 130-4 compared to 26.4 km/s and 25.9 km/s for the previous shots, respectively. Hence it is clear that the larger driver and its increased convergence of driver gas produce greater peak reservoir conditions, hence greater shock velocities at the diagnostic stations. Indeed, this shock velocity is the highest that has been obtained in the program to data, and as such represents a milestone in our progress.

Tabulated in Table 2 are the measured and calculated initial flow velocities for these four experiments. One

notes generally that the calculated flow velocity and the measured flow velocity differ with the measured values being lower than the calculations by 5-20 percent. This is probably within our ability to infer reservoir conditions at this point in time. The difficulty is threefold; 1, the equation of state for the driver gases at near megabar pressures is not precisely known. 2, calculating the expected flow velocity requires assuming an expansion process from "known" reservoir conditions. As the reservoir conditions are not steady in time, the expansion process is not the simple process modeled in the calculation, i.e. steady flow expansion to the channel entrance where the flow Mach number equals 1 followed by an unsteady flow expansion along the channel. 3, as the expansion processes are not simple, but contain upstream and downstream running shock and rarefaction waves[7], seeking a single representative number for initial shock speed may not be realistic in practice.

The flow velocity histories for the four shots are shown in Figure 9. Four points are worth noting. The conical driver of Shot 130-1 has a slightly higher peak flow velocity than either 130-2 or 130-2, but the decay rate is much greater and the total flow time is less than one-half of that from 130-2 or 3. The argon and xenon shots with the 17 cm. diameter driver produce very similar flow

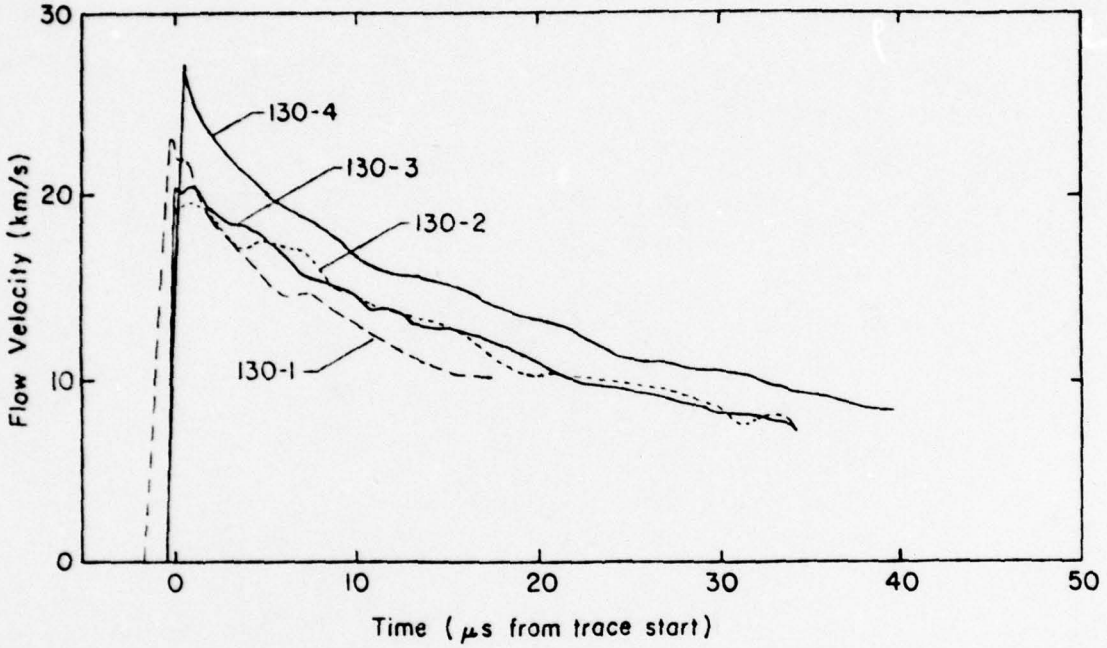

Figure 9 Comparison of Flow Velocities

velocity histories, both in absolute value of velocity and flow time.

The 30 cm. diameter driver of 130-4 gives substantially greater flow velocities; indeed the highest peak obtained in our research to date. These velocities are greater at any given time and are maintained to approximately 40-45 microseconds in time. The efficacy of the larger diameter driver is clearly apparent from this trace. However, the decay of the channel is greater than expected. The decline in velocity implies that the higher reservoir conditions are not being maintained as long as would have been expected with the additional mass of working gas produced by the larger driver.

These points suggest the possibility that other previously unsuspected phenomena may be limiting test flow time both for the small driver as well as the large. A prime candidate is the premature "pinching off" of the flow at the channel entrance by distortions of the entrance region by the very high reservoir pressures. This type of behavior has been observed by others, for example, the computer experiments of the Voitenko compressor performed by Brown and Lohmann of LLL[8]. They observed that at very high reservoir pressures, well in excess of the yield stresses

in the reservoir wall material, the reservoir end wall near the channel is extruded in the channel entrance region, "pinching off" the outflow. Even if the flow is not completely blocked, a "nozzle" is created at the channel entrance requiring the gases expand further in a steady expansion before shifting to an unsteady expansion. As the steady expansion is less efficient in translating pressure into velocity than the unsteady expansion for flow Mach numbers greater than unity, less shock velocity is obtained for a given reservoir condition. A discussion of this subtle but not commonly appreciated point is given in Reference 7.

This problem, and modifications to the reservoir--channel transition area to counter it, will be addressed in future work.

3.3 Expanded Plasma Electrical Properties

The electrical conductivity of the gas in the channel is of key interest in this research. Not only are precise values of conductivity presently impossible to obtain theoretically due to the complex nonideal nature of the plasmas, but the measurements also include significant scatter in results, both from similar instrumentation and between different measurement techniques.

For example, Figure 10 shows electrical conductivity determined from an eddy current gage (described earlier) and that determined from examining the V-I characteristics of the loaded generator section. One notes that the conductivities vary by about a factor of two with the eddy current gage giving the higher values.

The conductivity results from Shot 130-2 are shown in Figure 11. In this case, two electrical conductivity gages were used, one upstream and one downstream of the load section (see Figure 4). The gages gave similar results with the downstream gage giving generally slightly higher values. One also notes that the conductivity histories are maintained in time better than 130-1 as would be expected from examining the particle velocity histories of the two shots.

As previously, one also notes that the values determined from the load section are lower by about 50 percent.

The electrical conductivity data for Shot 130-3 are given in Figure 12. In this shot, 3 eddy current gages were used to obtained conductivity in addition to the values determined from the load resistance, and self-excited generator sections. The locations of the 5 different

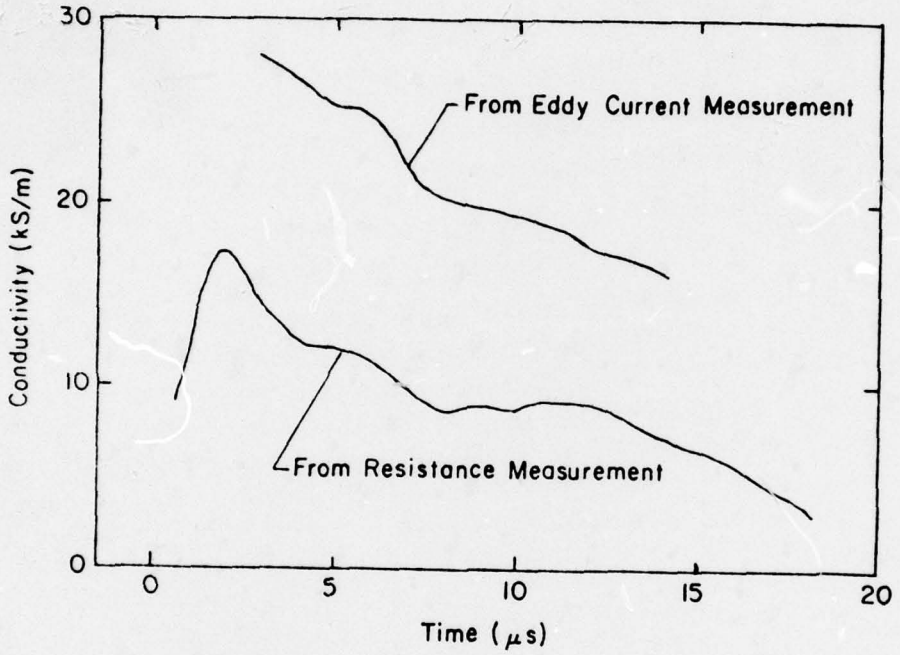

Figure 10 Channel Plasma Conditions Measured on Shot 130-1

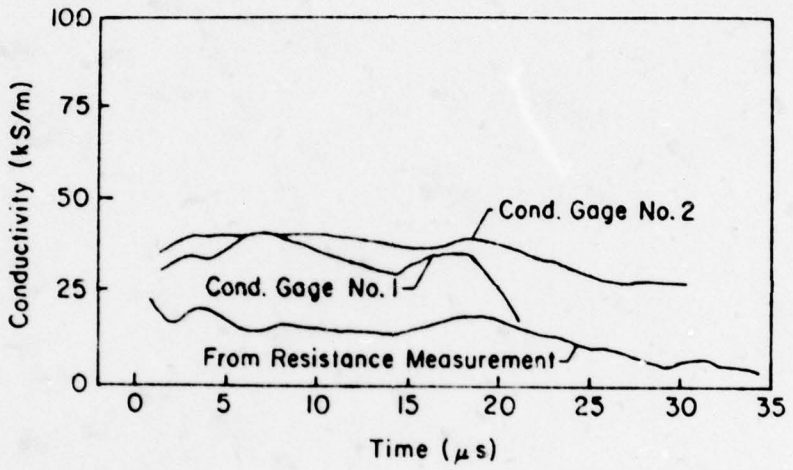

Figure 11 Results of Plasma Properties Measurements on Shot 130-2

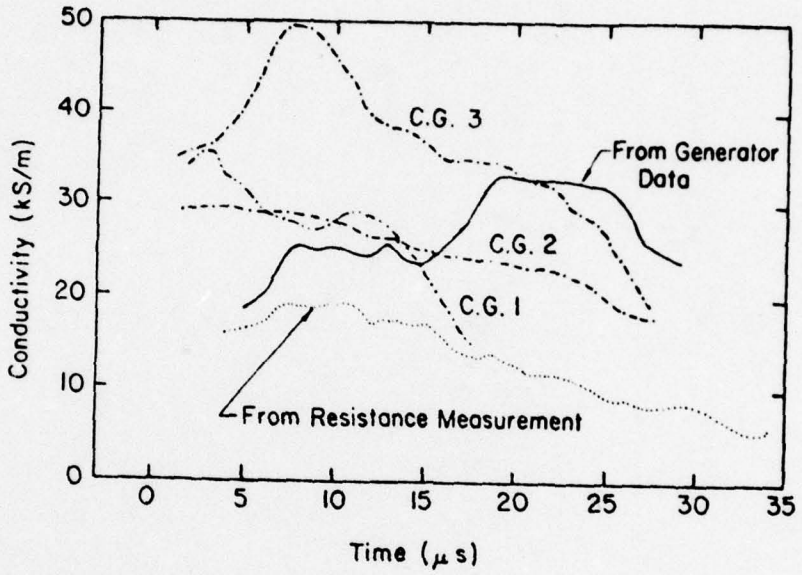

Figure 12 Plasma Conductivity from Various Data Sources (Shot 130-3)

measurements can be determined from Figure 6 and should not be dismissed in accounting for the different conductivity values. The time values shown are from the start of each trace and are at different absolute times. A plot of the values reordered to a laboratory time scale shows some interesting effects. For example, in Figure 13 we note that conductivity appears generally to be increasing as the flow progresses downstream and has a generally decreasing trend with time at a given measurement station.

We also note that the conductivity measurements based on the load measurements and self-excited generator measurements show an increase in conductivity for the first few (< 5) microseconds. If this is a transient effect caused by say, electrode/gas processes, then the agreement in the shape begins to look better. The last maxima in the generator derived trace remains unexplained. As the traces for 130-4 are unreliable late in the flow, no additional data is available for comparison.

We expect that more might be gleaned from this data by an analysis of the various data channels microsecond by microsecond, and propose to use such a technique on future runs.

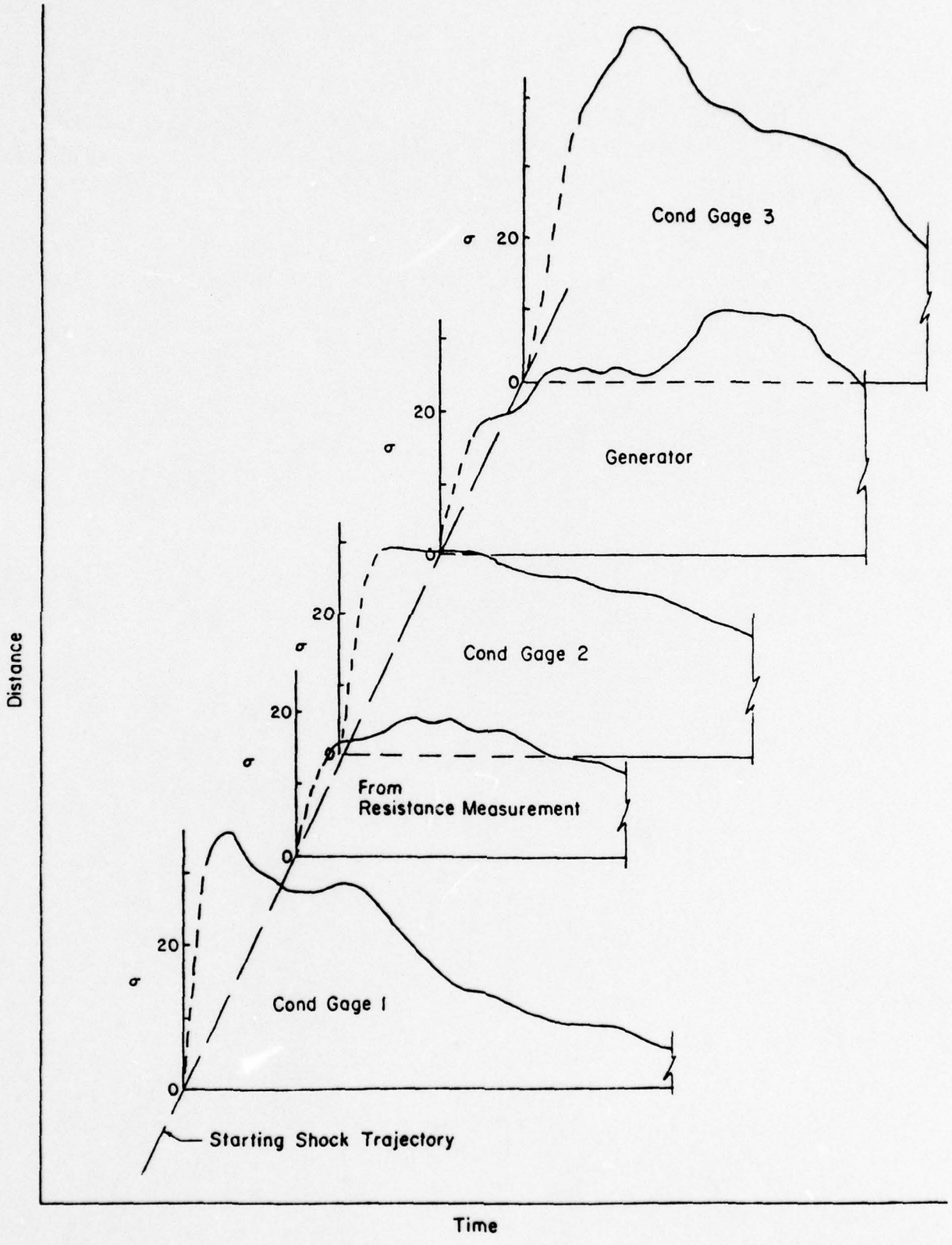

Figure 13 Plasma Conductivity from Various Sources Plotted versus Laborotory Time

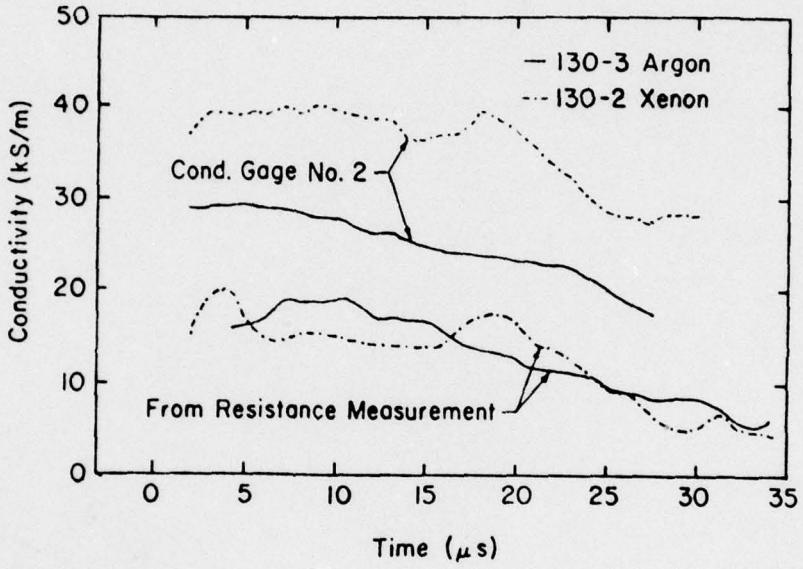

Figure 14 Conductivity Comparison for Xenon and Argon Shots (130-2, 130-3)

A side-by-side comparison of conductivity records between Shots 130-2 and 130-3 is shown in Figure 14 and provides another useful result. Conductivity, as measured by the eddy current conductivity gages, indicate a higher conductivity for xenon by about 30%. As the average conductivity determined by resistance measurements are comparable for the two experiments, this result suggests that possibly boundary layer effects, which are likely to be similar in the two cases, are responsible for lowering average conductivity.

The electrical conductivity histories for Shot 130-4 are shown in Figure 15. The values appear generally correct but the wide variation at later times suggests instrumentation problems. The first 10 microseconds for gage 1 appear reasonable as do the first 7 microseconds of gage 2 and first 5 microseconds of gage 3. Restricting attention to these times suggests the limited data to be reasonable. Again, the values obtained from the loaded generator are substantially lower than those measured by the eddy current gages.

3.4 Self-Excited MHD Generator Section

Additionally, Shots 130-3 and 130-4 were run with a self-excited MHD generator section on each. These diagnostic devices provide additional information on the flow.

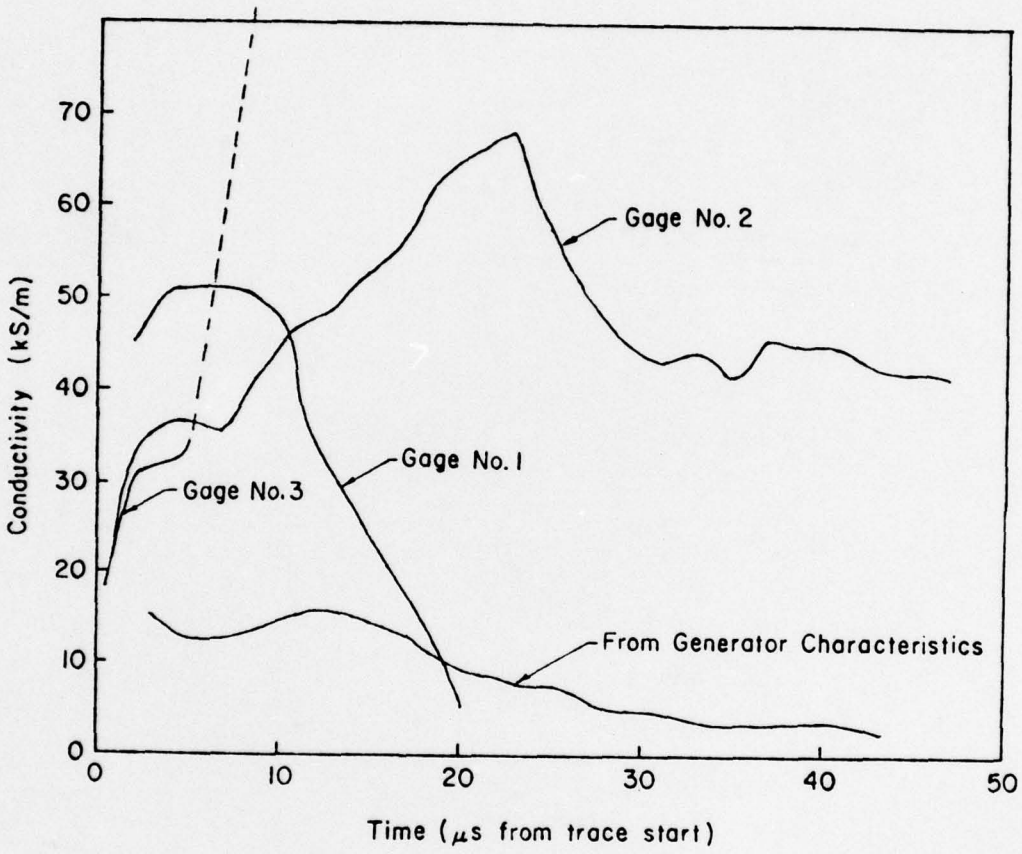

Figure 15 Electrical Conductivity Histories, Shot 130-4

For example, field coil data at the generator station for 130-3 are shown in Figure 16. Self-excitation is occurring throughout the entire pulse, as evidenced by increasing current and positive voltage. A short circuit occurs at 34μs, probably due to failure of the Mylar plastic insulation in the coil. Total magnetic field amplification during the pulse was 19 dB (a factor of 9). Initial increase was 1.3 dB/μs, falling to 0.4 dB/μs at the end of the pulse.

The MHD generator was analyzed for consistency by using measured plasma parameters to calculate performance, and then comparing them with observed values. The B-field magnitude was calculated from measured initial field, current, and B/I. This was combined with velocity to yield the open circuit Faraday voltage (Bub) shown in Figure 17.

Initially, at I = 0, the calculated open circuit voltage exceeds measured field coil voltage. This may be caused by internal inductance of the generator, forming an inductive voltage divider with the load. A value of 16 nanohenries agrees with the data, but is larger than theoretical estimates, which yield about 5 nanohenries. On the other hand, internal inductance of the load station had previously been determined to be 14 nanhenries. An alternate explanation is loading of the generator by eddy currents, expected

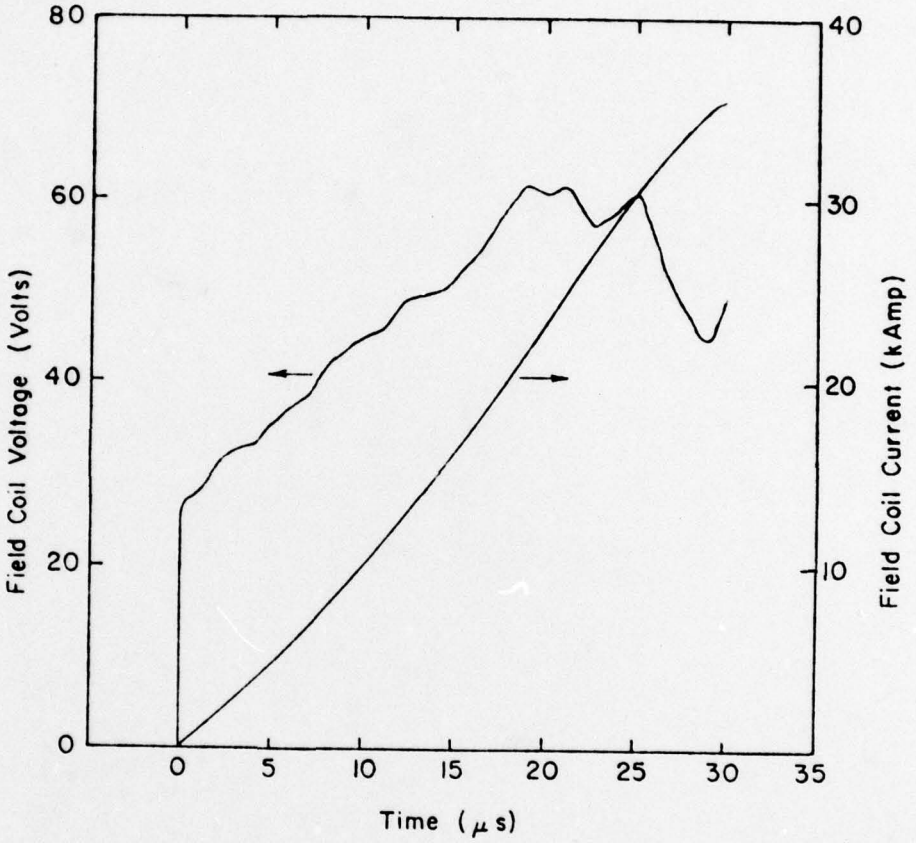

Figure 16 MHD Self-Excited Field Coil

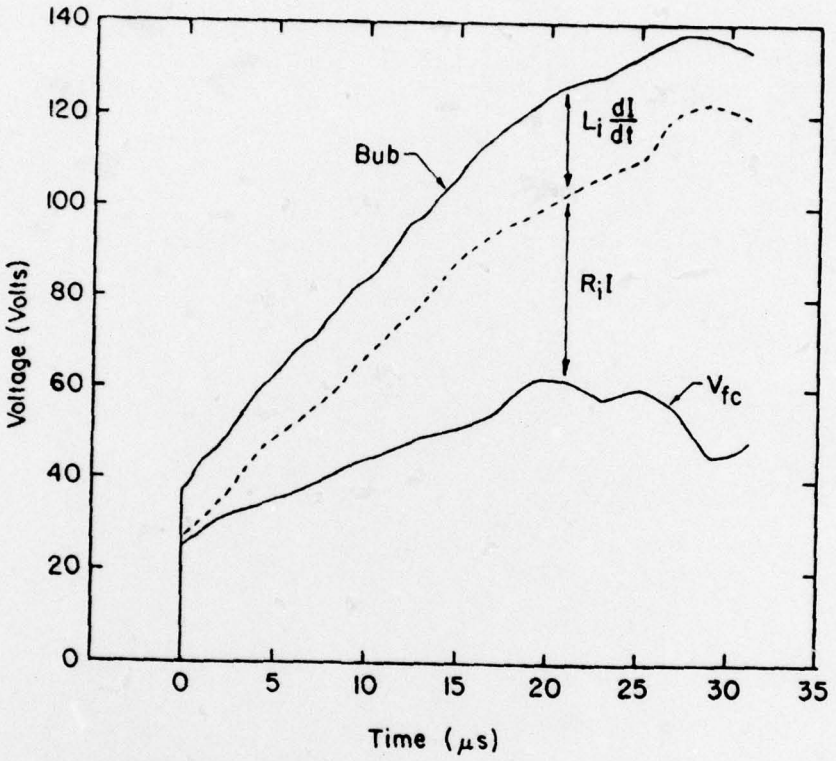

Figure 17 Estimate of Composite Voltage Drops in Generator

because of the very short coil length; this loading would act much like an inductive divider in the present experiment. Some reduction of open circuit Bub was expected, but the observed amount of about 33% appears excessive. Better design of the field coil assembly might well be able to reduce it to 15% or less.

The inductive drop in generator voltage was computed and is also shown in Figure 17. The remaining component of the voltage drop is that due to plasma resistance. By using this voltage drop together with the generator current, plasma resistance and conductivity were determined. The results of this analysis were previously shown together with the other conductivity measurements in Figure 12.

We note that the conductivity estimated from the MHD generator data is consistently higher than the values determined from upstream resistance measurements, and close to free-stream values obtained from eddy current measurements. It should be noted that CG#3 data may be suspect, since fabrication problems caused the shot configuration to differ from the calibration configuration (the coil was closer to the magnet, and the magnets were slightly further apart). Generally the MHD generator data agree reasonably well with the free-stream conductivity values.

The self-excited generator output is shown in Figure 18. Voltages in excess of 85 volts were reached. The observed drop in the voltage at 14 microseconds is probably an instrumentation artifact since its effect is not seen in the instantaneous magnetic field. A peak magnetic field of 0.65 Tesla was reached at 36 microseconds, an increase by a factor of 8.32 over the initial field, or 18.3 dB. This is essentially the same result as was obtained in run 130-3 with a smaller diameter driver.

The measured electrical conductivity determined from the generator characteristics was shown in Figure 15 and is noted to be improved somewhat over 130-3.

3.5 Field Amplification

Figure 19 is a plot of the self-excited field amplification of Shots 130-3 and 130-4. We note from the figure that the 50 percent longer time of the flow of 130-4 did not permit greater field amplification as the trajectory in field-time space is essentially the same as 130-3 with the exception that the absolute values of 130-4 are approximately 10% less than 130-3 at any given time.

The conclusion of this plot is, that longer test times by themselves will not increase field amplification significantly

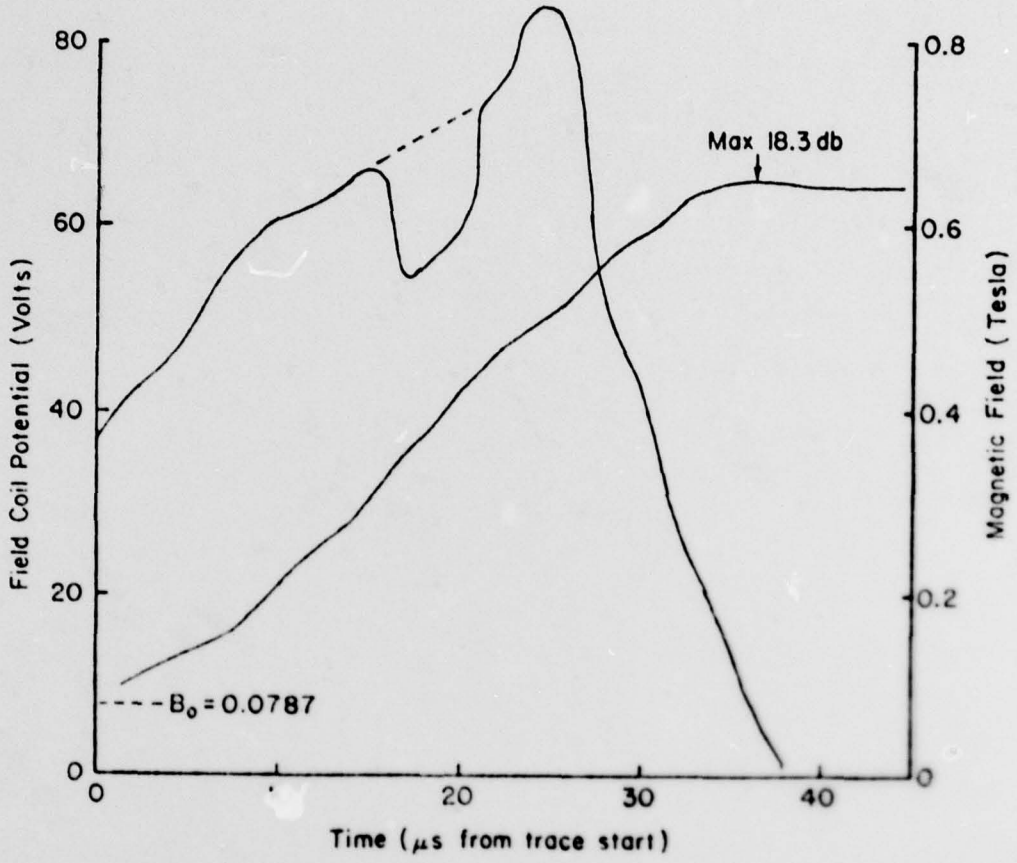

Figure 18 Self Excited Generator Potential and Field vs Time, Shot 130-4

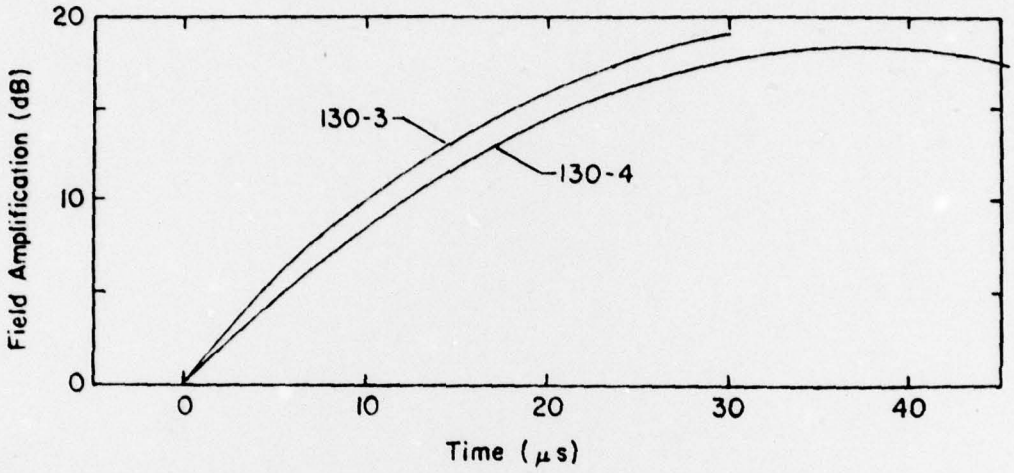

Figure 19 Comparison of Self-Excited Field Amplification

unless the rate of field amplification for early times in the flow are also improved. For example, if the initial enhancement rate of 130-3 of 1.3 dB/μsec could be maintained for 30 microseconds or greater, then a 40 dB improvement (factor of 10^2) increase in magnetic field could be achieved. For the present conditions the field amplification peaks out at 30 to 40 microseconds and the greater test time is not utilized to advantage. This demonstrates that future field enhancement gains must be obtained by simultaneously increasing flow velocity, conductivity and flow duration.

3.6 Summary of Conclusions

This new explosive plasma source can be distinguished from most other high-performance explosive devices, for example the disc driver or the Voitenko compressor, in that the geometry employed in the present device permits a far greater fraction of the gas tube processed initially by a single strong shock. In this way a higher average enthalpy plasma is obtained with the result that one obtains a higher conductivity ($\sigma \sim 38$ kS/m), and the conductivity remains high for a comparatively long period of time in the flow (>20μs).

The flow velocity-history of this plasma source was essentially identical when xenon was replaced by argon.

Bulk electrical conductivity of the argon was about 70% of the xenon values, and average values from resistance measurements, about the same.

The self-excited MHD generator worked well, and performed in accordance with theory based on measured field coil and plasma parameters. A maximum total gain of 19 dB was accomplished.

The measured electrical conductivities of the larger source are noted to be improved somewhat over the smaller, confirming that greater conductivities are possible using the larger diameter plasma source.

The evidence supports the premise that higher velocity flow in the channel can also be obtained by the larger diameter source, but that the higher reservoir conditions may also cause a "pinching off" of the channel entrance and a premature reduction of flow conditions.

This last effect may be ameliorated by simple geometry changes near the reservoir to channel transition and will be addressed in future experiments.

4. RECOMMENDATIONS

The progress and results of the four experiments designed, fired and analyzed in this period were very satisfying and suggest additional fruitful research.

We recommend a detailed analysis of the time history of the plasma source reservoir conditions including the effect of piston trajectory be made. We feel that by understanding the dynamics of this region we may well be able to tailor the reservoir dynamics to yield optimum conditions in the reservoir and hence downstream in the diagnostic channel.

Additionally, the premature closing of the diagnostic channel entrance, which was uncovered in the present work, may well have been a factor in all of the annular driver runs to date, both smaller driver diameter and large driver diameter. Amelioration of this effect may produce significant gains and should be investigated.

We recommend investigating a plasma source loaded with air, as the driver gas, as preliminary estimates suggest that the electrical conductivity of air at these very high densities may well be similar to that measured using argon and xenon. An experiment such as this confirming this hypothesis would be of interest to and have ramifications for other scientific areas of interest to the Navy.

We recommend investigating different configurations of conductivity gages to resolve the wide variation in measured conductivity, i.e. to determine if the variation is due to the variation of plasma properties with position in the channel or to experimental resolution, and a detailed comparison of the conductivity time histories for clues as to the details of the complex behavior of the flow.

And finally, we recommend additional effort to refine the self-excited generator diagnostic section including modeling of the output, in order to resolve the self-excited generator performance limit problem.

REFERENCES

1. Baum, Dennis W. et al, "Research on Nonideal Plasmas," Artec Associates Incorporated, Final Report 126, Navy Contract NR099-414/05-05-77 (473), May, 1978.

2. Gill, Stephen P. et al, "Explosive MHD Research," Artec Associates Incorporated, Annual Report 119, Navy Contract N00014-75-C-0822, April, 1976.

3. Baum, Dennis W. et al, "Development of High Energy Density Simulator," Artec Associates Incorporated, Final Report 120, Defense Nuclear Agency Contract DNA001-75-C-0271, December, 1976.

4. Mukherjee, D., "Nonideal Effects in Dense Argon and Xenon Plasmas," *Proceedings of First ONR Nonideal Plasma Workshop*, Pasadena, California, 14-15 November, 1978.

5. Kury, J. W. et al, "Metal Acceleration by Chemical Explosives," Fourth Symposium on Detonation, ONR, 1965.

6. Lee, E. et al, "JWL Equation of State Coefficients for High Explosives," University of California Lawrence Livermore Laboratory, UCID-16189, January, 1973.

7. Flagg, R. F., "A Theoretical Analysis of the Driver-Reservoir Method of Driving Hypersonic Shock Tunnels," Proceedings of the Fifth Shock Tube Symposium, USNOL 28-30 April, 1965.

8. Brown, P. S. et al, "Computational Studies of a Voitenko Compressor," University of California Lawrence Livermore Laboratory, UCRL-82010, November, 1978.

DISTRIBUTION LIST

	No. Copies
Office of Naval Research Power Program, Code 473 Arlington, Virginia 22217 Attn: J. A. Satkowski	3
Director, Naval Research Laboratory Washington, D.C. 20375 Attn: Code 2627	6
Defense Documentation Center Building 5, Cameron Station Alexandria, Virginia 22314	12
Office of Naval Research Branch Office 1030 East Green Street Pasadena, California 91106 Attn: E. T. Florance	1
University of Colorado Joint Institute for Laboratory Astrophysics Boulder, Colorado 80309 Attn: Dr. Arthur V. Phelps	1
Naval Surface Weapons Center Dahlgren, Virginia 22448 Attn: Dr. Frank Rose, Code OF-12	1
NASA Ames Research Center Moffett Field, California 94035 Attn: Mr. Robert Dannenburg	1
Director, Naval Research Laboratory Plasma Physics Division, Code 7770 Washington, D.C. 20375 Attn: Peter J. Turchi	1
Army Corps of Engineers P.O. Box 1600 Huntsville, Alabama 35807 Attn: Franklin R. Smith, Code ED-FR	

STD Corporation
P.O. Box C
Arcadia, California 91006
Attn: Dr. David Oliver 1
Mr. Clint Bangerter 1

University of Florida
Department of Nuclear Engineering Sciences
Gainesville, Florida 32601
Attn: Prof. R. T. Schneider 1

University of Florida
Department of Engineering Sciences
Gainesville, Florida 32601
Attn: Prof. Horst Wilhelm 1

Headquarters
Defense Nuclear Agency
Washington, D.C. 20305
Attn: John Farber 1

University of Nevada
Desert Research Institute System
Reno, Nevada 89507
Attn: Prof. S. Winterberg 1

Artec Associates Inc.
26046 Eden Landing Road
Hayward, California 94545
Attn: Dr. Dennis W. Baum 1
Dr. Stephen P. Gill 1
Dr. Deb Mukherjee 1
Dr. Robert F. Flagg 1

General Electric Company
Manager, MHD Programs
Valley Force Space Center
P.O. Box 8555
Philadelphia, Pennsylvania 19101
Attn: Dr. Bert Zauderer 1

University of Arizona
Head, Department of Planetary Sciences
Tucson, Arizona 85721
Attn: Prof. W. B. Hubbard 1

Lawrence Livermore Laboratory
H - Division
Livermore, California 94550

Attn:	Dr. Hugh E. Dewitt	1
	Dr. F. J. Rogers	1
	Dr. Harold Grabowski	1
	Dr. Marvin Ross	1
	Dr. Richard More	1

University of Rochester
Laboratory for Laswer Energetics
215 East River Road
Rochester, New York 14627

Attn:	Dr. Robert McCrory	1
	Dr. Stanley Skupsky	1

Los Alamos Scientific Laboratory
Los Alamos, New Mexico 87545

Attn:	Dr. Robert Malone	1
	Dr. Ping Lee	1
	Dr. John Shanner	1
	Dr. Walter Huebner	1
	Dr. Donald Dubois	1
	Dr. Max Fowler	1

University of Missouri
Physics Department
Rolla, Missouri 65401

Attn:	Prof. K. Nygaard	1